

**Crustal shearing at ductile-brittle transition**

E. Fazio et al.

This discussion paper is/has been under review for the journal Solid Earth (SE).  
Please refer to the corresponding final paper in SE if available.

# Polyphase evolution of a crustal-scale shear zone during progressive exhumation from ductile to brittle behaviour: a case study from Calabria, Italy

**E. Fazio, G. Ortolano, R. Cirrincione, A. Pezzino, and R. Visalli**

Università degli Studi di Catania, Dipartimento di Scienze Biologiche, Geologiche e Ambientali, Corso Italia 57, 95129 Catania, Italy

Received: 30 December 2014 – Accepted: 6 February 2015 – Published: 6 March 2015

Correspondence to: E. Fazio (efazio@unict.it)

Published by Copernicus Publications on behalf of the European Geosciences Union.

Title Page

Abstract

Introduction

Conclusions

References

Tables

Figures



Back

Close

Full Screen / Esc

Printer-friendly Version

Interactive Discussion



## Abstract

5 Mylonitic rocks involved within a polyphase crustal-scale shear zone, cropping out in the Aspromonte Massif (Calabria, Italy), has been investigated to reveal the meso- and micro-structural evolution (from ductile- to brittle-type deformation) occurred during exhumation trajectory. A relatively small area (about 4 km<sup>2</sup>) has been selected in the central-eastern part of the massif to constrain the sequence of the structural features from the earliest ones (Hercynian in age), almost totally obliterated by a pervasive mylonitic foliation (plastic regime), up to recent ones, consisting of various sets of veins typical of semibrittle to brittle regime. The former ductile evolution was followed by  
10 a compressive thin-skinned thrusting stage developed during the Apennine phase of the Alpine Orogeny, interested by a second brittle stage, consistent with the switching from compressive to extensional tectonics. This last stage accompanied the final exhumation process causing the activation of regional scale normal faults, which partly disarticulated previous mylonitic microstructures. A suite of oriented specimens were collected and analyzed to complete the deformational history already recognized in  
15 the field. Quartz *c* axis orientation patterns confirm the greenschist facies conditions of the former ductile exhumation stage with a dominant top-to-NE sense of shear. Microstructural investigations highlighted the progressive development from plastic- to brittle-type structures, allowing to constrain each step of the multistage exhumation history, and to establish the relative timing of the stress field variation causing thrusting and subsequent normal faulting. Obtained results support a continue compressional exhumation of this sector since the opening of Tyrrhenian basin (10 Ma).

## 1 Introduction

25 Crustal-scale shear zones are commonly rooted in the middle to lower crust. They evolve over a considerable period of time exhibiting a complex variety of fault-rocks microstructures, thus potentially becoming a good tool to unraveling the changes

## Crustal shearing at ductile-brittle transition

E. Fazio et al.

Title Page

Abstract

Introduction

Conclusions

References

Tables

Figures



Back

Close

Full Screen / Esc

Printer-friendly Version

Interactive Discussion



## Crustal shearing at ductile-brittle transition

E. Fazio et al.

Title Page

Abstract

Introduction

Conclusions

References

Tables

Figures



Back

Close

Full Screen / Esc

Printer-friendly Version

Interactive Discussion



in the deformation mechanisms during progressive deformation often associated to exhumation (Ramsay, 1980). For this reason, it is common to observe a sequential evolution of the deformation passing from crystal-plastic microstructures to brittle fracturing (Simpson, 1986). The reconstruction of this sequence can allow to unravel the exhumation history of originally deep seated crystalline basement rocks constraining rheological behavior, variation in the stress-field orientation as well as *PT* conditions of shearing activity.

In this view is inserted the present work that would to be analyze the rheology, the kinematics and the *PT* conditions of the different evolutionary steps of the Montalto Shear Zone (MSZ) (Cirrincione et al., 2009). MSZ is indeed a beautiful example of a continuum of deformation from ductile- to brittle-type with a lot of transitional stages located in the central-eastern part of the Aspromonte Massif. This massif (Cirrincione et al., 2013), together with the Peloritani Mountains Belt (Cirrincione et al., 2012) represent the most shortened southernmost segment of the Calabrian Peloritani Orogen (CPO) (Pezzino et al., 2008). The evolution of this orogenic segment occupies a key role in the kinematics of the entire orogen, unraveling the Oligocene-Miocene opening of Mediterranean back-arc basins, which developed within an overall collisional tectonic setting. In this scenario several tectonic models were proposed (e.g. Rosenbaum et al., 2002 and reference therein), which are mostly associated to the syn-orogenic retreat of the subducting plate, justifying the observed drifting phenomena of the present-day peri-Mediterranean thrust belts. These models attempt to explain the exhumation mechanisms, such as syn-convergent extension (Heymes et al., 2010) or extrusion by flow channeling (Pezzino et al., 2008; Cirrincione et al., 2008a), which operated during the uplifting process, involving the southern CPO crystalline basement rocks.

Within these contrasting views our work aims to be deep the evolution of the structural features from ductile- to brittle-types behaviors, analyzing in detail the relationships between meso- and micro-structural features of the MSZ. The study of the sequential evolution of the MSZ can contribute indeed to constrain the kinematics and the stress-field orientation variation, occurring during the different stages of the





type metamorphism which has not been detected into the overlying APU. According to Cirrincione et al. (2008b), this is supported by pre-mylonitic relics found both in the APU and MPU suggesting distinct tectono-metamorphic evolutions. The first ones indicate a clockwise polyphase evolution at relatively HT/LP regime, ascribable to the entire Hercynian metamorphic cycle, whereas the second ones, seem to be affected by an early Alpine metamorphism at HP/LT peak conditions. The evolution of the overlapping tectonics along a regional detachment shear-zone, replaced the original mylonitic fabrics, causing the shortening of the chain and the folding of the original main shear-plane. This last structural evolution further evolved in the more superficial conditions with the activation of thrusting structures, fractally distributed at different scales with formation of conjugate low-angle fractures (Ortolano et al., 2015). The more recent evolution of CPO is characterized by the activation of NE–SW brittle extensional fault system in response to a change from the collisional processes to an extensional tectonics, which took place in the upper Miocene (Monaco et al., 1996). In this time occurs the Tyrrhenian basin opening linked with the coexistence of extensional and compressional phenomena responsible for the structuring of the whole Apennine-Maghrebian Orogen (Finetti and Del Ben, 1986). Simultaneously, the NW subduction of the Ionian oceanic crust through a slab sinking mechanism took place (Malinverno and Ryan, 1986) accompanied by the formation of a regional strike-slip tectonics averagely oriented NW–SE, known as South Tyrrhenian System (Finetti et al., 1996; Lentini et al., 2002; Guarnieri et al., 2002), locally still active in the central and eastern part of the CPO. Finally, the last stages of the CPO structural evolution are marked by a currently active extensional Quaternary tectonics which resulted in an extensive regional uplift and in the sequential activation of seismogenic normal fault systems. The latter extend from the current Calabrian Tyrrhenian edge up to the Hyblean Plateau crossing the Strait of Messina and forming the so-called Siculo-Calabrian Rift Zone (SCRZ) (Monaco and Tortorici, 1995, 2000; Tortorici et al., 1995). In the study area, the different fault segments of the SCRZ system extend up to several hundred of kilometers and are characterized by a prevalent NNE–SSW trend typically observed

**Crustal shearing at ductile-brittle transition**

E. Fazio et al.

Title Page

Abstract

Introduction

Conclusions

References

Tables

Figures



Back

Close

Full Screen / Esc

Printer-friendly Version

Interactive Discussion











discussed. In this context a suite of oriented specimens were collected from the same outcrop (see Fig. 2 for location and Fig. 7 for petrographic features). Usually two orthogonal thin sections were prepared and analyzed for each sample: one was cut parallel to the stretching lineation ( $X$  direction,  $L_{1A}$ ), the other was cut orthogonal with respect the lineation, both of them are perpendicular to the mylonitic foliation ( $XY$  plane,  $S_{3A}$ ).

The uppermost tectono-metamorphic unit outcropping in the study area, the Silo Unit (SU), is essentially made by Variscan low-grade shales and phyllites (Crisci et al., 1982; Bonardi et al., 1984; Fazio et al., 2015). The typical assemblage is given by Qtz + Wm + Pl + Chl + Bt + Ilm (Fazio et al., 2012, 2015). Since this unit was not affected by the shear zone its microstructural features will be not further treated in the following.

The intermediate Aspromonte-Peloritani unit (APU) is composed essentially by middle crustal biotite paragneisses and leucocratic augen gneisses with minor amphibolites, mica schists and marbles. Rocks belonging to the APU collected for this study are highly foliated ultramylonites, mylonites, and cataclasites (Figs. 7 and 8) showing good examples of brittle deformation overprinting an earlier ductile fabric. The main assemblage is given by Qtz + Pl + Kfs + Bt + Wm + Chl + Ep + Grt + Tur developed at about 540 °C and 0.45 GPa during the syn-shear metamorphic episode followed by a retrograde metamorphism characterised by thermobaric condition ranging from 500 °C–0.5 GPa to 450 °C–0.25 GPa ( $PT$  estimates after Cirrincione et al., 2008b). Thin sections cut parallel to NE–SW show a top to the NE sense of shear (Fig. 8). At the sub-centimetric scale it is possible to observe ultramylonite levels interbedded with mylonite and cataclasite portions of the same rock depicting at places a cataclastic flow. Spectacular intrafolial oblique folds with disharmonic appearance, sometimes resembling micro-sheath folds, have also been recognized (Fig. 9, CD thin section of SDA3). Mica fish are widespread. Quartz occurs as ribbons, sometimes showing micro-folds with axial planes sub-parallel to the mylonitic foliation ( $S_{3A}$ ). Quartz domains are also characterized by smaller recrystallized grains forming

SED

7, 909–955, 2015

## Crustal shearing at ductile-brittle transition

E. Fazio et al.

Title Page

Abstract

Introduction

Conclusions

References

Tables

Figures

⏪

⏩

◀

▶

Back

Close

Full Screen / Esc

Printer-friendly Version

Interactive Discussion





grainsize with respect to the APU rocks, the earlier ductile features are fully obliterated. White mica fish are diffuse. Garnet grains are very rounded suggesting erosion during transitional ductile-brittle shear regime; ribbon-like quartz (SGR + GBM, undulatory extinction) showing internal oblique foliation are diffusely occurring; pre-kinematic PI with core-rim (dusty-limpid).

## 4.2 Quartz LPO

On a suite of collected samples the lattice preferred orientation (LPO) of recrystallized quartz grains was inferred by the CIP method (computer integrated polarization microscopy; Heilbronner, 2000), widely adopted in microstructural analysis of mylonitic rocks (e.g. Heilbronner and Tullis, 2006; Menegon et al., 2008; Fazio et al., 2010; Pennacchioni et al., 2010). In particular, eight domains of oriented specimens have been investigated in order to retrieve information about the orientation of the optical  $c$  axes of recrystallized quartz grains. Quartz  $c$  axis patterns are shown on Fig. 10.

The dominant crystallographic distribution of quartz  $c$  axis is represented by a diffuse basal ( $a$ ) slip system (Fig. 10a–h) suggesting a main recrystallization episode happened under shear strain at greenschist facies condition (Schmid and Casey, 1986; Stipp et al., 2002). At a lesser extent the rhomb ( $a$ ) and prism ( $a$ ) slip systems are also developed (Fig. 10a, e and g). Minor prism ( $c$ ) slip system has been also registered (samples SDA1, SDA11; Fig. 10a and e).

In one case a late discordant vein (Fig. 10h'') crosscutting the earlier mylonitic foliation displacing ribbon-like quartz levels (Fig. 10h–h') has also been investigated. Results, thus not correlated with the shear zone activity but undoubtedly to a subsequent episode, show a peculiar pattern with a maxima between the  $X$  and  $Z$  directions and a general rhombic symmetry linked to the specific orientation of maximum stress during crystals growth into the opening vein (Fig. 10h'').

SED

7, 909–955, 2015

## Crustal shearing at ductile-brittle transition

E. Fazio et al.

Title Page

Abstract

Introduction

Conclusions

References

Tables

Figures

⏪

⏩

◀

▶

Back

Close

Full Screen / Esc

Printer-friendly Version

Interactive Discussion



### 4.3 Qtz deformation mechanisms

The dynamic recrystallization of quartz domains testifies the activation and protracting of deformation by means of dislocation creep mechanisms which produced characteristic fabrics in the Montalto sheared rocks. In particular, prevalent subgrain rotation recrystallization (SGR), with minor bulging (BLG) and sporadic grain boundary migration (GBM), has been recognized as the main recrystallization process.

Recrystallization microstructures typically developed in crustal scale shear zone affecting quartz-feldspar-mica bearing rocks denoting quartz intracrystalline plasticity were observed. Oblique foliation developed at about 15° with respect the shear zone boundaries (c surfaces) is delineated by new recrystallized smaller grains (average diameter ca. 50 microns) suggesting a dominant SGR recrystallization process (Fig. 11a). This fabric has been observed thorough almost all samples collected from the Montalto shear zone (Fig. 10b–g). Larger grains forming ribbons are elongated with major axis parallel to the main foliation (long axis about 500 microns, Figs. 10b, d, e, and 11b). They exhibit optically visible subgrains and show at their borders tiny recrystallized grains typical of SGR (core and mantle texture, Fig. 11c).

Syntectonic recrystallization of quartz probably has proceeded towards the last exhumation phases of the shear zone, during progressive cooling, causing the overprint of lower temperature fabric over higher temperature ones. This causes that mylonites pass through the BLG–SGR transition, which has been estimated to occur approximately at 280 °C (Dunlap et al., 1997), 400 °C (Stipp et al., 2002). Moreover fracturing also occurs (Fig. 7e) in alternation to dynamic recrystallization as a response to the rising of local differential stress up to the magnitude of confining pressure (Kuster and Stockert, 1999). Interestingly mica flakes occurring at the boundary of these fragmented quartz domains, at the end of opening veins show local kinking (Fig. 11d) suggesting that deformation (intracrystalline plasticity) has continued after the fracture propagation.

SED

7, 909–955, 2015

## Crustal shearing at ductile-brittle transition

E. Fazio et al.

Title Page

Abstract

Introduction

Conclusions

References

Tables

Figures

⏪

⏩

◀

▶

Back

Close

Full Screen / Esc

Printer-friendly Version

Interactive Discussion



## 4.4 Qtz paleopiezometry

Paleopiezometry calculation based on the mean grain size of a recrystallized quartz-rich domain from an highly deformed mylonite was also performed (SDA3 sample, Fig. 12). This was useful to infer the differential stress ( $\Delta\sigma$ ) active during the shearing deformational phase (Poirier, 1985). To this aim a grain boundary map was obtained from a stack of three CIP misorientation images adopting the Lazy grain boundary macro (Heilbronner, 2000) with the Image SXM software (Barrett, 2010). The selected domain containing 3542 particles can be considered statistically valid to infer differential stress (Herwegh et al., 2011). Applying an empirical equation (Stipp and Tullis, 2003) corrected by Holyoke et al. (2010), considering the mean grain size of 42 microns, a differential stress ( $\Delta\sigma$ ) of  $0.25\beta$  GPa was inferred.

Since the value of differential stress is known and the deformation mechanisms correlated with dislocation creep regime which produced characteristic related microstructures (BLG, SGR) were recognized, the strain rate ( $\dot{\epsilon}$ ) can be retrieved by adopting a flow law equation (Bürgmann and Dresen, 2008) in the following form:

$$\dot{\epsilon} = A\sigma^n d^{-m} f_{\text{H}_2\text{O}} e^{\frac{(-Q+pV)}{RT}} \quad (1)$$

where  $A$  is a material constant,  $\sigma$  is the applied stress,  $n$  is the (power-law) stress exponent,  $Q$  is the activation energy,  $p$  is the pressure,  $V$  is the activation volume,  $T$  is the absolute temperature,  $R$  is the molar gas constant,  $d$  is the grain size,  $m$  is the grain-size exponent,  $f_{\text{H}_2\text{O}}$  is the water fugacity, and  $r$  is the fugacity exponent.

Our estimates are calibrated on the experimental data obtained for quartzite under wet conditions (Hirth et al., 2001), realistically approximating conditions of natural shear zones with associated mylonites (Stipp et al., 2002), by adopting values of  $A$ ,  $Q$ , and  $n$  as follows:  $6.30957 \times 10^{-12}$  ( $\text{MPa}^{-n} \text{s}^{-1}$ ),  $135\,000$  ( $\text{J mol}^{-1}$ ), and 4 respectively. Indeed, petrographical evidences confirm that hydrous minerals (e.g. muscovite) are constituents of syn-shearing assemblage.

SED

7, 909–955, 2015

### Crustal shearing at ductile-brittle transition

E. Fazio et al.

Title Page

Abstract

Introduction

Conclusions

References

Tables

Figures

◀

▶

◀

▶

Back

Close

Full Screen / Esc

Printer-friendly Version

Interactive Discussion



## Crustal shearing at ductile-brittle transition

E. Fazio et al.

Title Page

Abstract

Introduction

Conclusions

References

Tables

Figures

⏪

⏩

◀

▶

Back

Close

Full Screen / Esc

Printer-friendly Version

Interactive Discussion



In order to obtain reliable estimates for water saturated conditions, appropriate water fugacity values have been selected (Tödheide, 1972) by taking into account the thermal range deduced from quartz *c* axis patterns, which is comprised between 350 and 550 °C, being basal (*a*) the dominant active slip system. These thermal estimates are also consistent with those proposed by previous studies (Cirrincione et al., 2008b) who also determined pressure conditions for the Montalto shear zone in the range 0.3–0.45 GPa.

We then calculated the strain rate values at the following *PT* shearing conditions: *P* (0.45 GPa); *T* (550 °C), for which a value of  $f_{\text{H}_2\text{O}} = 4.82$  GPa has been selected (Tödheide, 1972). The strain rate ( $\dot{\epsilon}$ ) found for the Montalto shear zone (SDA3 sample) is  $3.21 \times 10^{-12}$  ( $\text{s}^{-1}$ ), which is in agreement with typical values of actively deformed regions ( $10^{-12}$  to  $10^{-15}$   $\text{s}^{-1}$ ; Behr and Platt, 2011) and natural shear zone ( $10^{-9}$  to  $10^{-13}$   $\text{s}^{-1}$ ; Bürgmann and Dresen, 2008). Nevertheless the above mentioned *PT* conditions were attained during the initial phase of shearing but deformation has continued up to shallower crustal conditions. For this reason we also made a further paleopiezometry calculation attempting to estimate the last phase of the same shearing event at lower *PT* conditions (0.30 GPa and 350 °C). Such calculation, considering a value of  $f_{\text{H}_2\text{O}} = 1.35$  GPa (Tödheide, 1972), gives a strain rate value rate ( $\dot{\epsilon}$ ) of  $1.62 \times 10^{-15}$  ( $\text{s}^{-1}$ ).

### 4.5 Brittle microstructures

Besides cataclastic flow, which has been recognized in a couple of samples (SDA14, SDA10), three sets of joints/veins have been recognized (sample SDA1, Figs. 11–13):

1. Millimeter-thick lentoid shaped epithermal veins (Fig. 11), usually paraconcordant with respect the mylonitic foliation, consisting of polygonal aggregates of K-feldspar (adularia, Ad), at places truncating both micaceous and quartz rich domains delineating the mylonitic foliation ( $S_{3A}$ ).

**Crustal shearing at ductile-brittle transition**

E. Fazio et al.

2. Thinner massive veins (Fig. 11a–d) characterized by walls with a high concentration of opaque minerals (Fe-oxides) at high angle with respect the mylonitic foliation ( $S_{3A}$ ) filled by feldspar, chlorite, and quartz. Sealing quartz is sometimes characterized by undulatory extinction, testifying that deformation was still active at subsolidus conditions. This second set of tiny veins (Fig. 11d), truncating both the early mylonitic microfabric ( $S_{3A}$ ) and the first set of veins, sometimes appears as suture joint (teeth-saw profile) resembling stylolites, coherent with the same sigma1 orientation active during the first vein opening, oriented parallel to the main foliation. Possibly this set of joint is also related to the final stage of the  $D_{5A}$  brittle episode.

3. The last microstructures related to the fragile regime (Figs. 11–14) are breccias, pseudotachylytes and close fractures. The latter crosscut at an average angle of  $60^\circ$  the mylonitic foliation causing its displacement (Fig. 7f). Sometimes such microcracks produce fibrous opening veins filled by biotite and sericite (Fig. 12) or sporadically also quartz veins (Fig. 13) suggesting that both of them are related to an extensional tectonic event ( $D_{6A}$ ) that became active at relatively deep seated conditions ( $T > 250^\circ\text{C}$ ;  $P > 0.3\text{ GPa}$ ) at least during its initial phase.

## 5 Discussion and timing of deformational phases

The relationships between ductile and fragile structures are here described to highlight the possible evolution of the shearing MSZ activity through the reconstruction of the overprinting and dispersion relations among the different evolutionary stages, controlled sequentially the exhumation trajectory of the Aspromonte Massif crystalline basement units (Fig. 15, Table 2). From the integrated analysis at the field- and thin section-scale of the two deep seated outcropping units (i.e. APU and MPU) the following possible tectonic evolution can be delineated.

[Title Page](#)[Abstract](#)[Introduction](#)[Conclusions](#)[References](#)[Tables](#)[Figures](#)[Back](#)[Close](#)[Full Screen / Esc](#)[Printer-friendly Version](#)[Interactive Discussion](#)

## Crustal shearing at ductile-brittle transition

E. Fazio et al.

Title Page

Abstract

Introduction

Conclusions

References

Tables

Figures



Back

Close

Full Screen / Esc

Printer-friendly Version

Interactive Discussion



The most developed deformational phase ( $D_{3A}$ ), here obliterating most of the previous structures, is typical for the development of structures during the evolution of a non-coaxial plastic-type deformation with formation of a weakly to strongly mylonitic foliation ( $S_{3A}$ ) and a stretching lineation ( $L_{1A}$ , parallel to the tectonic transport direction, see SDA3 thin section, Figs. 8 and 9) and a layering given by alternating micaceous and quartz-feldspar rich domains. Syn- to post-mylonitic asymmetric microfolds of quartz layers are widespread. Mica fish, S-C-C' textures, ribbon like quartz, book-shelf feldspar are characteristic microstructures of this stage. Ultramylonites develop during this tectonic phase.

The second phase is related to the ductile-brittle transition coeval with the shear zone uplifting (a possible change and/or decrease of the main shear plane inclination occurred at this time). The tectonic transport ( $D_{4A}$ ) causes overpressure in the pile nappes edifice with development of a set of veins (joints) overprinting mylonites (Fig. 15, see SDA1 thin section). Two sets of veins are characteristic of this phase: syntaxial veins ( $V_{1A}$  – sigma1 oriented parallel  $w/r$  to  $S_{3A}$ ) of blocky feldspar and quartz (similar to the Ad + Ab + Qtz “Alpine veins” of Rossi et al., 2005, possibly related to high K-Na fluid circulation) usually para-concordant with respect to the mylonitic foliation. Large grain size of such sealing crystals are due to a rising temperature effect associated with a considerable enrichment of fluids pressure. These veins ( $V_{1A}$  veining episode, Table 2) sometimes are not fractured by subsequent veins ( $V_{2A}$  stylolite-like veins) probably for a mineral-rheology related contrast of competence between surrounding micaceous matrix constituting the host rock and the vein itself. Adularia crystallization (Rossi et al., 2005) into paraconcordant veins is possibly linked to high-K-Al-Si fluid circulation (upflow zones – most likely Ad takes place under dynamic conditions that are characteristic of an open system such as fault fissures carrying geothermal fluid – i.e. a hydrothermal K-feldspar precipitated by the geothermal fluid, and forming incrustations on fissured wall rocks). Probably such epithermal veins ( $V_{1A}$ ) opened at ca. 300 °C, after Steiner, 1970). Sigmoidal recrystallized quartz observed in one sample (SDA1) into a quartz-rich domain is considered coeval with this veining

## Crustal shearing at ductile-brittle transition

E. Fazio et al.

Title Page

Abstract

Introduction

Conclusions

References

Tables

Figures



Back

Close

Full Screen / Esc

Printer-friendly Version

Interactive Discussion



stage (Fig. 10e). Indeed the surrounding quartz domain is characterized by a classical low temperature quartz  $c$  axis pattern (Fig. 10), whereas the new quartz grains, with a different crystallographic orientation, have tails sub-parallel to the main foliation which should be coincident with the sigma 1 direction at the time of recrystallization coevally with respect the Apennine thrusting phase ( $D_{5A}$ ). The  $V_{1A}$  set of veins has been interpreted as syn-tectonic hydraulic fractures parallel to the sigma1 direction probably coeval with the  $D_{4A}$  tectonic phase responsible for the verging to isoclinal folding of  $S_{3A}$  evolving to the thrusting phase ( $D_{5A}$ ) responsible for the low angle faults (LAF) visible at the outcrop scale. Indeed, fluid pressure may increase during thrust sheet emplacement. Then a network of stylolite-like massive veins ( $V_{2A}$  – sigma1 oriented parallel  $w/r$  to  $S_{3A}$ ) sub-coeval with the previous ones develops. They often appear as suture joints at high angle with respect  $S_{3A}$ . Elevated fluid pressure, which led to fracturing, dilation, and fault initiation, coupled with progressive decreasing temperature, resulted in the transition from ductile folding to brittle thrusting (e.g. Gibson, 1985). Changing physical conditions probably reflect erosional unroofing during uplift and late Apennine thrust sheet emplacement.

The subsequent tectonic collapse of the chain ( $D_{6A}$ ) favored the variation of the sigma 1 orientation, changing from sub-horizontal to sub-vertical (switching of sigma1 with sigma3), and the development of both  $V_{3A}$  veins at microscale and of normal faults connected to the last brittle episode ( $D_{6A}$ ) at the regional scale, causing the recent horst and graben structure of the entire Aspromonte Massif crystalline edifice (Fig. 3g). At the onset of the maximum stress orientation switching, characterized by an increasing vertical loading, a set of veins marked this stage ( $V_{3A}$  – sigma1 oriented perpendicular  $w/r$  to  $S_{3A}$ ): tiny fuzzy antitaxial fibrous veins (Chl, Wm, Bt) with Fe-oxides at walls, and massive veins filled by large quartz crystals crosscutting at high angle ribbon like quartz parallel to the mylonitic foliation. These microstructures are related to the syn- to post-exhumation vertical loading of the entire basement edifice marking also a possible connection with the recognized meso-structural scale high angle faults (HAF) (Fig. 3).

## Crustal shearing at ductile-brittle transition

E. Fazio et al.

Title Page

Abstract

Introduction

Conclusions

References

Tables

Figures



Back

Close

Full Screen / Esc

Printer-friendly Version

Interactive Discussion



The third phase ( $D_{6A}$ ) has developed under the classic brittle regime s.s. Two brittle sub-stages can be distinguished: (first stage) cataclastic flow and breccias overprinting mylonites and development of pseudotachylyte (Pst) crosscutting mylonitic layers (parallel to the mylonitic foliation), connecting the  $V_{3A}$  set of veins with large quartz grains. Sometimes injectites have been recognized; (second stage – sigma1 oriented perpendicular  $w/r$  to  $S_{3A}$ ): high angle micro faults (jogs, dilation veins with microscale pull apart basin) with dip-slip or displacement visible at thin section scale suggesting a connection with mesostructural high angle faults (HAF).

## 6 Conclusions

The structural analysis conducted both at the meso- and micro-scale allowed us to detect a complex tectono-metamorphic evolution of the Montalto shear zone, evolving from ductile to brittle regime, passing through the ductile-brittle transition. Several evidences, like microstructures, mineral rheology, quartz LPO pattern, suggest for this crustal scale shear zone a mylonitic stage at greenschist facies condition (up to lower amphibolite facies, Cirrincione et al., 2008b) with associated typical ductile strain features like quartz ribbons, mica fish, rounded porphyroclasts, oblique foliation, isoclinal folds with recrystallized grains of quartz with their longest axis sub parallel to the fold axial surface. Moreover, the study of the crystallographic orientation of recrystallized quartz grains of selected domains by the CIP method permitted us to confirm greenschist facies thermal range of the shear zone activity as well as to gain information about the sense of shear in the nowadays geographic coordinates, giving an average tectonic transport vergency towards NE.

Concerning the quartz LPO, the dynamically recrystallized grains develop a broad maximum near the  $Z$  direction compatible with a dominant basal  $\langle a \rangle$  slip occurred at about 300–350 °C (greenschist facies conditions) with subordinate rhomb  $\langle a \rangle$  and prism  $\langle a \rangle$  slip systems developed under 450–550 °C (amphibolite facies conditions). The geologically constrained dislocation creep flow law of Hirth et al. (2001) for wet quartz

## Crustal shearing at ductile-brittle transition

E. Fazio et al.

Title Page

Abstract

Introduction

Conclusions

References

Tables

Figures

⏪

⏩

◀

▶

Back

Close

Full Screen / Esc

Printer-friendly Version

Interactive Discussion



has given realistic results in the calculation of strain rate in the Montalto sheared rocks. Indeed when considering the shearing conditions (temperatures and stresses) of the studied area, the mylonites should have deformed at strain rates ( $\dot{\epsilon}$ ) of  $3.21 \times 10^{-12}$  to  $1.62 \times 10^{-15}$  ( $\text{s}^{-1}$ ) for differential stress ( $\Delta\sigma$ ) of 0.25 GPa estimated by paleopiezometry (Stipp and Tullis, 2003). These strain rate values inferred from quartz paleopiezometry can be considered to be realistic if compared to the geological literature data for crustal-scale shear zones.

At the transition between a typical ductile rock behavior and an initial fragile regime, a mixture of features belonging to the opposite finite strain products is observed. In particular the careful crosscutting relationships between several sets of veins at the microscale allowed us the whole tectonic history to be better constrained. Massive veins, related to fragile rock behavior, sealed with adularia, quartz (syntaxial vein) and biotite (antitaxial vein) suggesting thermal condition above 250 °C, referable to the ductile regime up to the ductile-brittle transition. The peculiar orientation of such veins, sub-parallel to the main mylonitic foliation, suggests that exhumation has developed fundamentally in a compressional stress field rather than in an extensional one. Up to this stage both meso- and micro-scale structures related to ductile regime as well as to transitional and semibrittle ones furnish evidences of a continue deformation developed in a compressional settings. Then characteristic brittle structures such as cracks, micro-faults, dilation veins and joints are superimposed on the clearly plastic deformational features acquired during early stages of the tectonic history. Such microstructural observations have their correlative features both at the meso- and mega-scale, especially regarding the low-angle faults (LAF) and high-angle faults (HAF) linked to the thrusting phase and the subsequent normal faulting of the entire Aspromonte Massif edifice, respectively.

We can conclude that the whole structural dataset provide evidences for an articulated, but relatively continued polyphase evolution of the investigated fault-rocks involved within the MSZ evolution, which has been delineated thanks to a careful geological and structural analysis supported by microscopic observations. Results are

concordant with an exhumation activity substantially developed in a compressional regime operating from the Oligocene-Miocene deepest mylonitic shearing activity (Alpine phase,  $D_{3A}$ – $D_{4A}$ ) and continued up the former stages of the thin skinned Apennine evolutionary stages (Apennine phase,  $D_{5A}$ ). Our observations suggest then that the switching from compressional to extensional regime, can be ascribed only to the still active final evolutionary stage (i.e. Apennine phase,  $D_{6A}$ ) causing the activation of a dip-slip tectonics which brought to the formation of the present-day horst and graben structure of the Aspromonte Massif.

**The Supplement related to this article is available online at doi:10.5194/sed-7-909-2015-supplement.**

*Acknowledgements.* We thank Renée Heilbronner for making available the CIP facilities at the University of Basel. Daniele Castelli is greatly acknowledged for making available devices to take microphotographs at the Earth Science Department of Turin University.

## References

- Angi, G., Cirrincione, R., Fazio, E., Fiannacca, P., Ortolano, G., and Pezzino, A.: Metamorphic evolution of preserved Hercynian crustal section in the Serre Massif (Calabria-Peloritani Orogen, southern Italy), *Lithos*, 115, 237–262, 2010.
- Barrett, S. D.: Image SXM, University of Liverpool, available at: <http://www.ImageSXM.org.uk>, last access: December 2014, 2010.
- Behr, W. M. and Platt, J. P.: A naturally constrained stress profile through the middle crust in an extensional terrane, *Earth Planet. Sc. Lett.*, 303, 181–192, 2011.
- Bonardi, G., Compagnoni, R., Messina, A., and Perrone, V.: Riequilibrazioni metamorfiche di probabile età alpina nell'Unità dell'Aspromonte – Arco Calabro Peloritano, *Rendiconti della Società Italiana di Mineralogia e Petrologia*, 39, 613–628, 1984.

SED

7, 909–955, 2015

## Crustal shearing at ductile-brittle transition

E. Fazio et al.

Title Page

Abstract

Introduction

Conclusions

References

Tables

Figures

◀

▶

◀

▶

Back

Close

Full Screen / Esc

Printer-friendly Version

Interactive Discussion



## Crustal shearing at ductile-brittle transition

E. Fazio et al.

Title Page

Abstract

Introduction

Conclusions

References

Tables

Figures



Back

Close

Full Screen / Esc

Printer-friendly Version

Interactive Discussion



Bonardi, G., Compagnoni, R., Del Moro, A., Messina, A., and Perrone, V.: Riequilibrizioni tettonico-metamorfiche Alpine dell'Unità dell'Aspromonte, Calabria Meridionale, Rendiconti della Società Italiana di Mineralogia e Petrologia, 42, p. 301, 1987.

Bürgmann, R. and Dresen, G.: Rheology of the lower crust and upper mantle: evidence from rock mechanics, geodesy and field observations, *Annu. Rev. Earth Pl. Sc.*, 36, 531–567, doi:10.1146/annurev.earth.36.031207.124326, 2008.

Cirrincone, R., Fazio, E., Fiannacca, P., Ortolano, G., Pezzino, A., and Punturo, R.: Petrological and microstructural constraints for orogenic exhumation modelling of HP rocks: the example of southern Calabria Peloritani Orogen (Western Mediterranean), in: *GeoMod 2008, Third International Geomodelling Conference, Firenze, 22–24 September 2008*, *Boll. Geof. Teor. Appl.*, 49, 141–146, 2008a.

Cirrincone, R., Ortolano, G., Pezzino, A., and Punturo, R.: Poly-orogenic multi-stage metamorphic evolution inferred via P–T pseudosections: an example from Aspromonte Massif basement rocks (Southern Calabria, Italy), *Lithos*, 103, 466–502, doi:10.1016/j.lithos.2007.11.001, 2008b.

Cirrincone, R., Fazio, E., Fiannacca, P., Ortolano, G., and Punturo, R.: Microstructural Investigation of Naturally Deformed Leucogneiss from an Alpine Shear Zone (Southern Calabria – Italy), *Pure Appl. Geophys.*, 166, 995–1010, 2009.

Cirrincone, R., Fazio, E., Heilbronner, R., Kern, H., Mengel, K., Ortolano, G., Pezzino, A., and Punturo, R.: Microstructure and elastic anisotropy of naturally deformed leucogneiss from a shear zone in Montalto (southern Calabria, Italy), *Geological Society of London, Sp. Publ.*, 332, 49–68, 2010.

Cirrincone, R., Fazio, E., Ortolano, G., Pezzino, A., and Punturo, R.: Fault-related rocks: deciphering the structural–metamorphic evolution of an accretionary wedge in a collisional belt, NE Sicily, *Int. Geol. Rev.*, 54, 940–956, 2012.

Cirrincone, R., Fazio, E., Fiannacca, P., Ortolano, G., Pezzino, A., Punturo, R., Romano, V., and Sacco, V.: The Alpine evolution of the Aspromonte Massif: constraints for geodynamic reconstruction of the Calabria-Peloritani Orogen, *Geological Field Trips*, 5, 1–73, 2013.

Crisci, G. M., Donati, G., Messina, A., Russo, S., and Perrone, V.: L'Unità superiore dell'Aspromonte. Studio geologico e petrografico, *Rendiconti della Società Italiana di Mineralogia e Petrologia*, 38, 989–1014, 1982.

Dunlap, W. J., Hirth, G., and Teyssier, C.: Thermomechanical evolution of a ductile duplex, *Tectonics*, 16, 983–1000, 1997.

**Crustal shearing at ductile-brittle transition**

E. Fazio et al.

[Title Page](#)[Abstract](#)[Introduction](#)[Conclusions](#)[References](#)[Tables](#)[Figures](#)[⏪](#)[⏩](#)[◀](#)[▶](#)[Back](#)[Close](#)[Full Screen / Esc](#)[Printer-friendly Version](#)[Interactive Discussion](#)

Fazio, E., Cirrincione, R., and Pezzino, A.: Estimating P-T conditions of Alpine-type metamorphism using multistage garnet in the tectonic windows of the Cardeto area (southern Aspromonte Massif, Calabria), *Miner. Petrol.*, 93, 111–142, doi:10.1007/s00710-007-0216-2, 2008.

5 Fazio, E., Cirrincione, R., and Pezzino, A.: Garnet crystal growth in sheared metapelites (southern Calabria – Italy): relationships between isolated porphyroblasts and coalescing euhedral crystals, *Period. Mineral.*, 78, 3–18, 2009.

Fazio, E., Punturo, R., and Cirrincione, R.: Quartz *c* axis texture mapping of mylonitic metapelite with rods structures (Calabria, southern Italy): clues for hidden shear flow direction, *J. Geol. Soc. India*, 75, 171–182, 2010.

10 Fazio, E., Casini, L., Cirrincione, R., Massonne, H. J., and Pezzino, A.: P-T estimates for the metamorphic rocks of the Stilo Unit (Aspromonte Massif, Calabria) and correlations with analogue Sardinian Variscan crystalline complexes, Special meeting of French and Italian Geological Societies “Variscan 2012”, 22–23 May 2012, Sassari, Italy, *Geologie de la France*, 1, 111–113, 2012.

15 Fazio, E., Cirrincione, R., and Pezzino, A.: Tectono-metamorphic map of the south-western flank of the Aspromonte Massif (southern Calabria-Italy), *Journal of Maps*, 11, 85–100, 2015.

20 Fiannacca, P., Williams, I. S., Cirrincione, R., and Pezzino, A.: Crustal contributions to late Hercynian peraluminous magmatism in the Southern Calabria-Peloritani Orogen, Southern Italy: petrogenetic inferences and the Gondwana connection, *J. Petrol.*, 49, 1497–1514, 2008.

Finetti, I. and Del Ben, A.: Geophysical study of the Tyrrhenian opening, *B. Geofis. Teor. Appl.*, 28, 75–155, 1986.

25 Finetti, I. R., Lentini, F., Carbone, S., Catalano, S., and Del Ben, A.: Il sistema Appennino Meridionale – Arco Calabro – Sicilia nel Mediterraneo Centrale: studio geologico geofisico, *B. Soc. Geol. Ital.*, 115, 529–559, 1996.

Gibson, R. G.: Ductile-to-brittle transition in shear during thrust sheet emplacement, Southern Appalachian thrust belt, *J. Struct. Geol.*, 7, 513–525, 1985.

30 Grohmann, C. H. and Campanha, G. A. C.: OpenStereo: open source, cross-platform software for structural geology analysis, Presented at the AGU 2010 Fall Meeting, 15 December, San Francisco, CA, 2010.

## Crustal shearing at ductile-brittle transition

E. Fazio et al.

Title Page

Abstract

Introduction

Conclusions

References

Tables

Figures



Back

Close

Full Screen / Esc

Printer-friendly Version

Interactive Discussion



- Guarnieri, P., Carbone, S., and Di Stefano, A.: The Sicilian orogenic belt, a critical tapered wedge?, *Italian Journal of Geosciences*, 121, 221–230, 2002.
- Heilbronner, R.: Optical orientation imaging, in: *Stress, Structure and Strain: a volume in honour of Win D. Means*, edited by: Jessell, M. and Urai, J., *Journal of the Virtual Explorer, Electronic Edition*, 2, 9, doi:10.3809/jvirtex.2000.00012, 2000.
- Heilbronner, R. and Tullis, J.: Evolution of *c* axis pole figures and grain size during dynamic recrystallisation: results from experimentally sheared quartzite, *J. Geophys. Res.*, 111, B10202, doi:10.1029/2005JB004194, 2006.
- Herwegh, M., Linckens, J., Ebert, A., Berger, A., and Brodhag, S. H.: The role of second phases for controlling microstructural evolution in polymineralic rocks: a review, *J. Struct. Geol.*, 33, 1728–1750, 2011.
- Heymes, T., Monie, P., Arnaud, N., Pecher, A., Bouillin, J. P., and Compagnoni, R.: Alpine tectonics in the Calabrian–Peloritan belt (southern Italy): new 40Ar/39Ar data in the Aspromonte Massif area, *Lithos*, 114, 451–472, 2010.
- Hirth, G., Teyssier, C., and Dunlap, W. J.: An evaluation of quartzite flow laws based on comparisons between experimentally and naturally deformed rocks, *Int. J. Earth Sci.*, 90, 77–87, 2001.
- Kuster, M. and Stockhert, B.: High differential stress and sublithostatic pore fluid pressure in the ductile regime-microstructural evidence for short-term post-seismic creep in the Sesia Zone, Western Alps, *Tectonophysics*, 303, 263–277, 1999.
- Lentini, F., Carbone, S., Di Stefano, A., and Guarnieri, P.: Stratigraphical and structural constraints in the Lucanian Apennines (southern Italy): tools for reconstructing the geological evolution, *J. Geodyn.*, 34, 141–158, doi:10.1016/S0264-3707(02)00031-5, 2002.
- Malinverno, A. and Ryan, W. B. F.: Extension in the Tyrrhenian Sea and shortening in the Apennines as a result of arc migration driven by sinking of the lithosphere, *Tectonics*, 5, 227–245, doi:10.1029/TC005i002p00227, 1986.
- Menegon, L., Pennacchioni, G., Heilbronner, R., and Pittarello, L.: Evolution of quartz microstructure and *c* axis crystallographic preferred orientation within ductilely deformed granitoids (Arolla Unit, Western Alps), *J. Struct. Geol.*, 30, 1332–1347, doi:10.1016/j.jsg.2008.07.007, 2008.
- Monaco, C. and Tortorici, L.: Tectonic role of ophiolite-bearing terranes in the development of the Southern Apennines orogenic belt, *Terra Nova*, 7, 153–160, doi:10.1111/j.1365-3121.1995.tb00684.x, 1995.

## Crustal shearing at ductile-brittle transition

E. Fazio et al.

Title Page

Abstract

Introduction

Conclusions

References

Tables

Figures



Back

Close

Full Screen / Esc

Printer-friendly Version

Interactive Discussion



- Monaco, C. and Tortorici, L.: Active faulting in the Calabrian arc and eastern Sicily, *J. Geodyn.*, 29, 407–424, doi:10.1016/S0264-3707(99)00052-6, 2000.
- Monaco, C., Tortorici, L., Nicolich, R., Cernobori, L., and Costa, M.: From collisional to rifted basins: an example from the southern Calabrian arc (Italy), *Tectonophysics*, 266, 233–249, doi:10.1016/S0040-1951(96)00192-8, 1996.
- Ortolano, G., Cirrincione, R., and Pezzino, A.: P–T evolution of Alpine metamorphism in the southern Aspromonte Massif (Calabria–Italy), *Schweiz. Miner. Petrog.*, 85, 31–56, 2005.
- Ortolano, G., Cirrincione, R., Pezzino, A., and Puliatti, G.: Geo-Petro-Structural study of the Palmi shear zone: kinematic and rheological implications, *Rendiconti Online Società Geologica Italiana*, 29, 126–129, 2013.
- Ortolano, G., Cirrincione, R., Pezzino, A., Tripodi, V., and Zappalà, L.: Petro-structural geology of the Eastern Aspromonte Massif crystalline basement (southern Italy-Calabria): an example of interoperable geo-data management from thin section – to field scale, *Journal of Maps*, 11, 181–200, 2015.
- Pennacchioni, G., Menegon, L., Leiss, B., Nestola, F., and Bromiley, G.: Development of crystallographic preferred orientation and microstructure during plastic deformation of natural coarse-grained quartz veins, *J. Geophys. Res.*, 115, B12405, doi:10.1029/2010JB007674, 2010.
- Pezzino, A., Pannucci, S., Puglisi, G., Atzori, P., Ioppolo, S., and Lo Giudice, A.: Geometry and metamorphic environment of the contact between the Aspromonte–Peloritani Unit (Upper Unit) and Madonna dei Polsi Unit (Lower Unit) in the central Aspromonte area (Calabria), *B. Soc. Geol. Ital.*, 109, 455–469, 1990.
- Pezzino, A., Angi, G., Cirrincione, R., De Vuono, E., Fazio, E., Fiannacca, P., Lo Giudice, A., Ortolano, G., and Punturo, R.: Alpine metamorphism in the Aspromonte Massif: implications for a new Framework for the Southern Sector of the Calabria-Peloritani Orogen, Italy, *Int. Geol. Rev.*, 50, 423–441, 2008.
- Poirier, J. P.: *Creep of Crystals: High Temperature Deformation Processes in Metals, Ceramics, and Minerals*, Cambridge Univ. Press, Cambridge, UK, doi:10.1017/CBO9780511564451, 1985.
- Puglisi, G. and Pezzino, A.: Metamorphism in the central Aspromonte area: geological, mineralogical and petrogenetic relationships, *Period. Mineral.*, 63, 153–168, 1994.
- Ramsay, J. G.: Shear zone geometry: a review, *J. Struct. Geol.*, 2, 83–99, doi:10.1016/0191-8141(80)90038-3, 1980.



## Crustal shearing at ductile-brittle transition

E. Fazio et al.

**Table 1.** Total stations and structural data reported in the geological map of Fig. 2.

Unit	Station	$S_{1H}$	$B_{1H}$	$B_{2H}$	$S_{3A}$	$L_{1A}$	$B_{3A}$	$L_{2A}$	$B_{4A}$	LAF	HAF	Total_ Unit
SU	4	71	17	11	0	0	0	0	0	7	25	131
APU	29	0	0	0	873	79	23	32	16	47	136	1206
MPU	15	0	0	0	269	29	11	3	1	17	29	359
Total data	48	71	17	11	1142	108	34	35	17	71	190	1696

Title Page

Abstract

Introduction

Conclusions

References

Tables

Figures



Back

Close

Full Screen / Esc

Printer-friendly Version

Interactive Discussion



## Crustal shearing at ductile-brittle transition

E. Fazio et al.

**Table 2.** Synoptic scheme of deformational phases, associated structures and blastesis episodes.

Deformational events ( $D_n$ )	Associated structures		Metamorphic ( $M_n$ ) and veining ( $V_n$ ) episodes	Mineral assemblages	Notes
	Foliation	Lineation/ fold axis			
$D_{1H}$	$S_{1H}$	$B_{1H}$	$M_{1H}$	Qtz, Ilm, Wm, Bt, Pl, Grt, Sill, Kfs	Pre-shear assemblages (plastic behaviour)
$D_{2H}$	$S_{2H}$	$B_{2H}$	$M_{2H}$	Qtz, Pl, Chl, Wm, Bt, Grt, And	
$D_{1A}$	$S_{1A}$	$B_{1A}$	$M_{1A}$	Qtz, Pl, Chl, Wm, Bt, Grt, Ep, Amph, Ilm	
$D_{2A}$	$S_{2A}$	$B_{2A}$	$M_{2A}$	Qtz, Chl, Wm, Grt, Ilm	
$D_{3A}$	$S_{3A}$	$L_{1A}$	$M_{3A}$	Qtz, Wm, Chl, Pl, Grt, Bt, Czo, Amph, Tur	Syn-shear assemblage (plastic behaviour)
$D_{4A}$	$S_{4A}$	$L_{2A}, B_{3A}$	$M_{4A}$	Qtz, Wm, Pl, Chl, Czo	Syn- to post-shear assemblage (plastic behaviour)
	–	–	$V_{1A}$	Qtz, Ad, Pl	Syn-compressional assemblage (semibrittle behaviour)
$D_{5A}$	–	–	$V_{2A}$	Qtz, Chl, Wm	LAF – fracturing
$D_{6A}$	–	–	$V_{3A}$	Qtz, Bt, Wm, Chl	HAF – fracturing

[Title Page](#)
[Abstract](#)
[Introduction](#)
[Conclusions](#)
[References](#)
[Tables](#)
[Figures](#)
[Back](#)
[Close](#)
[Full Screen / Esc](#)
[Printer-friendly Version](#)
[Interactive Discussion](#)


## Crustal shearing at ductile-brittle transition

E. Fazio et al.

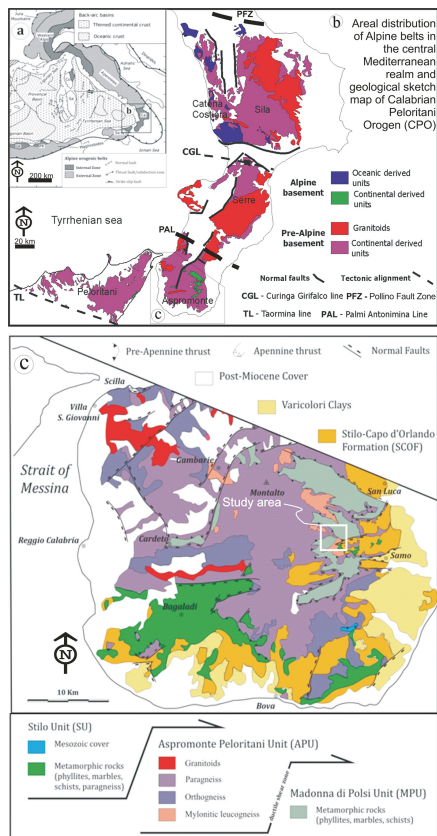


**Figure 1.** Synthesis of geological setting: **(a)** areal distribution of Alpine belt in the central Mediterranean realm; **(b)** geological sketch map of Calabrian Peloritani Orogen (CPO) (modified after Angi et al., 2010; Cirrincione et al., 2011); **(c)** geological sketch map of the Aspromonte Massif (after Pezzino et al., 1990, 2008; Ortolano et al., 2005; Fazio et al., 2008).

Title Page

Abstract

Introduction

Conclusions

References

Tables

Figures

◀

▶

◀

▶

Back

Close

Full Screen / Esc

Printer-friendly Version

Interactive Discussion

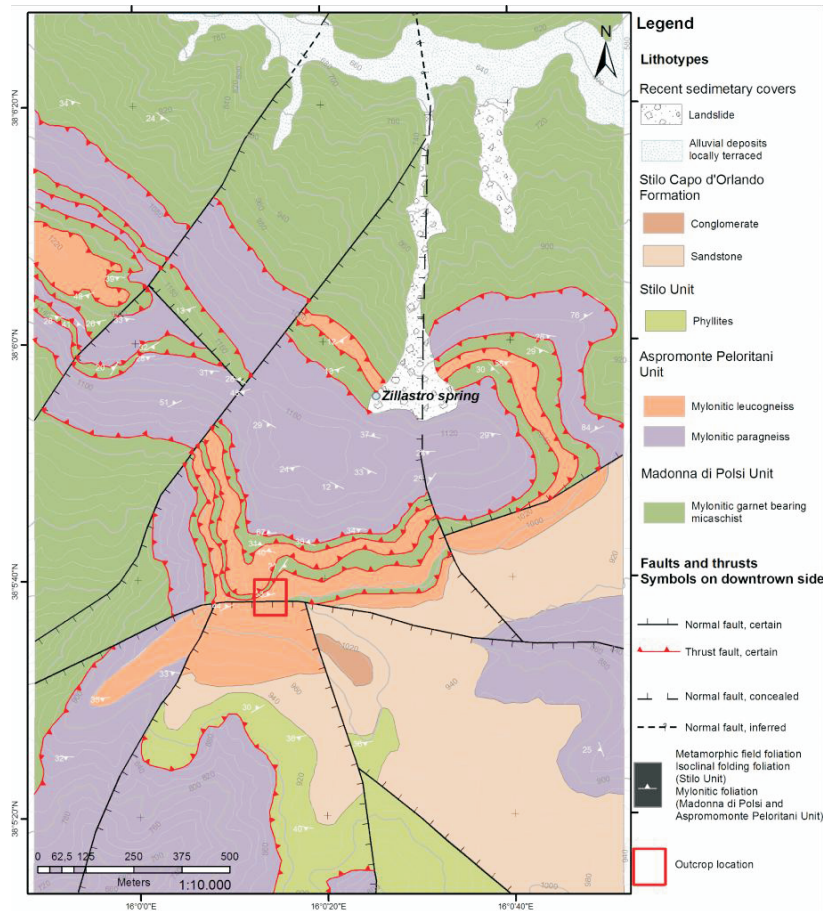


# SED

7, 909–955, 2015

## Crustal shearing at ductile-brittle transition

E. Fazio et al.



Title Page

Abstract

Introduction

Conclusions

References

Tables

Figures

◀

▶

◀

▶

Back

Close

Full Screen / Esc

Printer-friendly Version

Interactive Discussion



**Figure 2.** Detailed geo-structural map of the study area with outcrop location (scale 1 : 10 000).

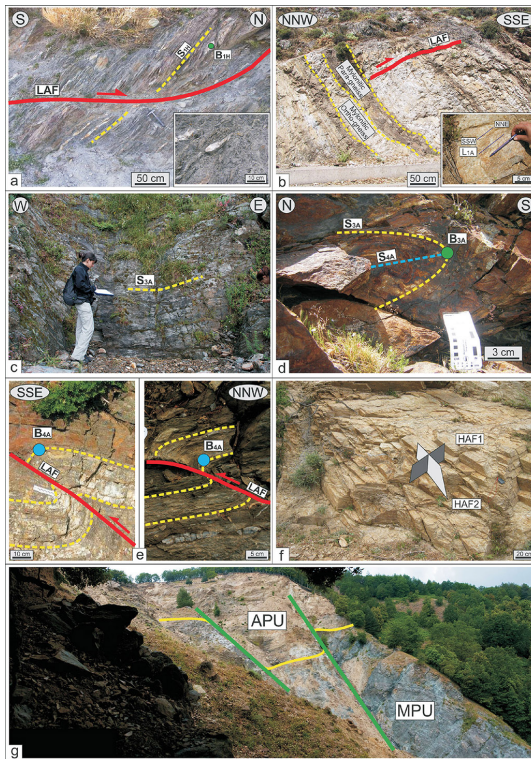


**Figure 3.** Outcrop features: **(a)** Stilo Unit phyllites; **(b)** alternance of mylonitic ortho- and paragneiss of the Aspromonte Peloritani Unit (inset showing detail of the stretching lineation); **(c)** Madonna di Polsi Unit mylonitic garnet bearing micaschist; **(d)** isoclinal post-mylonitic folding (mylonitic paragneiss of the APU); **(e)** asymmetric syn- $D_{5A}$  fold, evolving to brittle low angle fracture (LAF) both in the APU (to the left) and in the MPU rock-types (to the right); **(f)** conjugate high angle joint system in the mylonitic leucogneiss of the APU; **(g)** panoramic view of the early mylonitic contact between APU and MPU surfacing along the Zillastro landslide affected by the later brittle tectonics (see Fig. 2 for location).

**Crustal shearing at ductile-brittle transition**

E. Fazio et al.

Title Page	
Abstract	Introduction
Conclusions	References
Tables	Figures
◀	▶
◀	▶
Back	Close
Full Screen / Esc	
Printer-friendly Version	
Interactive Discussion	



**Crustal shearing at ductile-brittle transition**

E. Fazio et al.

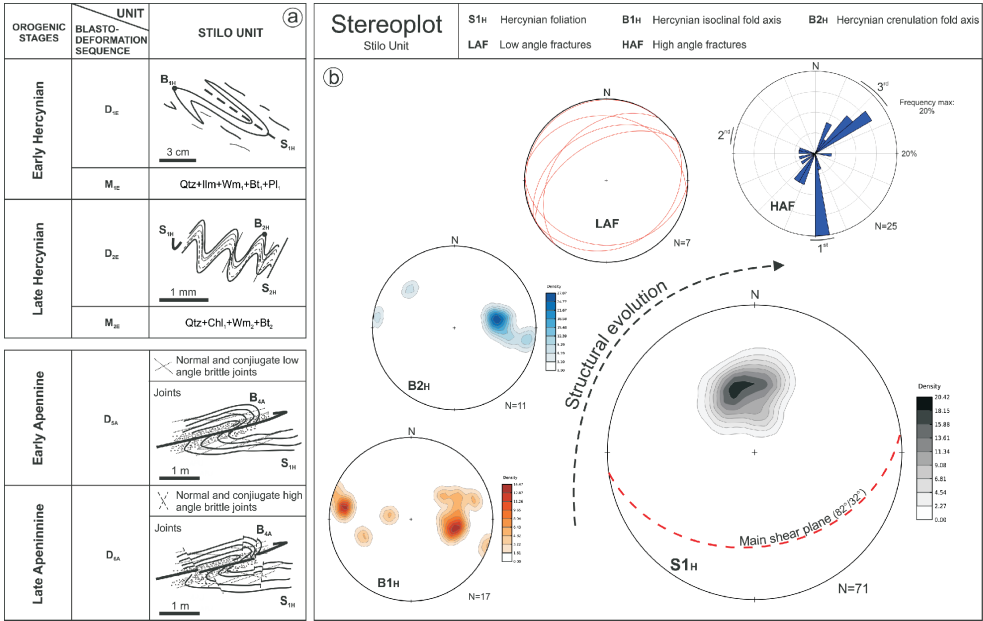


**Figure 4.** Schematic representation of Stilo unit (SU) structural evolution: **(a)** sequential blasto-deformational evolution with associated the orogenic stages from ductile to brittle sequence; **(b)** stereoplots of the main structural features observed in outcrops. *N* = number of measurements, 1st, 2nd, 3rd = high angle families hierarchy – longer segments corresponds to a greater number of data.

Discussion Paper | Discussion Paper | Discussion Paper | Discussion Paper | Discussion Paper

Title Page

Abstract Introduction

Conclusions References

Tables Figures

◀ ▶

◀ ▶

Back Close

Full Screen / Esc

Printer-friendly Version

Interactive Discussion



**Crustal shearing at ductile-brittle transition**

E. Fazio et al.

Title Page

Abstract

Introduction

Conclusions

References

Tables

Figures

◀

▶

◀

▶

Back

Close

Full Screen / Esc

Printer-friendly Version

Interactive Discussion

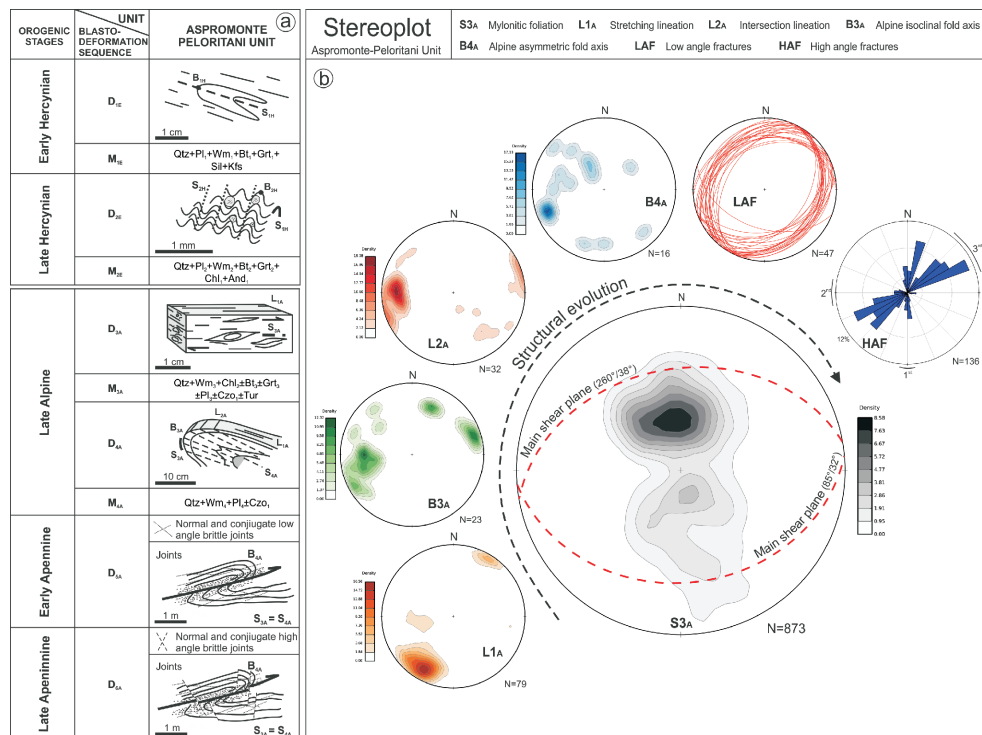


**Figure 5.** Schematic representation of Aspromonte-Peloritani unit (APU) structural evolution: **(a)** sequential blasto-deformational evolution with associated the orogenic stages from ductile to brittle sequence; **(b)** stereoplots of the main structural features observed in outcrops. *N* = number of measurements, 1st, 2nd, 3rd = high angle families hierarchy – longer segments corresponds to a greater number of data.



**Crustal shearing at ductile-brittle transition**

E. Fazio et al.

Title Page

Abstract

Introduction

Conclusions

References

Tables

Figures

◀

▶

◀

▶

Back

Close

Full Screen / Esc

Printer-friendly Version

Interactive Discussion

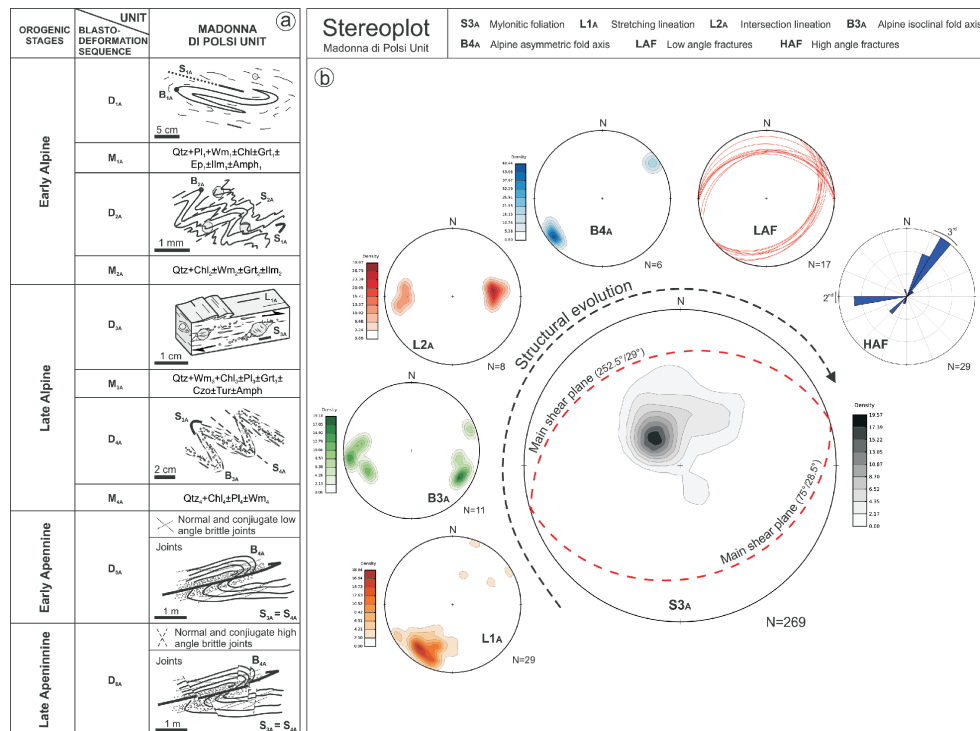


**Figure 6.** Schematic representation of Madonna di Polsi unit (MPU) structural evolution: **(a)** sequential blasto-deformational evolution with associated the orogenic stages from ductile to brittle sequence; **(b)** stereoplots of the main structural features observed in outcrops. *N* = number of measurements, 1st, 2nd, 3rd = high angle families hierarchy – longer segments corresponds to a greater number of data.



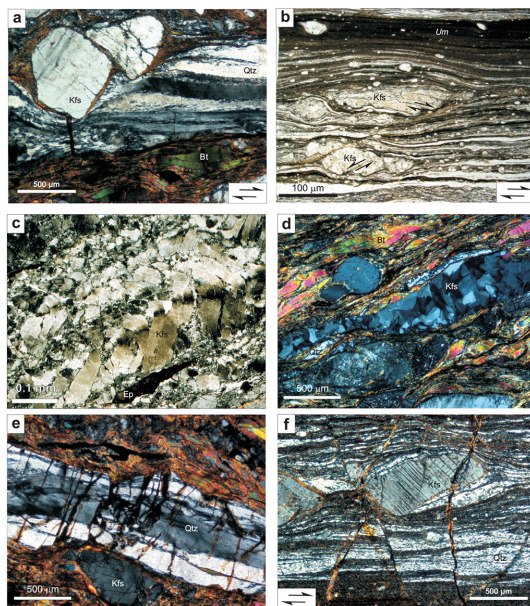


**Figure 7.** Microphotos: **(a)** classical view of an APU mylonite. The main foliation is characterized by alternating mica-rich (Bt “fish” shaped) and quartz-rich domains (ribbon-like) characterised by ondulose extinction, very fine grainsize (SGR-GBM) and a marked oblique foliation; **(b)** K-feldspar porphyroclasts showing domino-type structures (both synthetic and antithetic fractures are developed) floating into a very fine ultramylonite matrix (sample SDA13). Clasts have usually a flattened aspect, the elliptical shape is due to erosion of external edges during shear deformation. **(c)** Severely deformed pre-mylonitic K-feldspar showing intracrystalline plasticity associated with frictional sliding; **(d)** blocky adularia veins subparallel to the mylonitic foliation; **(e)** hydraulic fracturing of a quartz microlithon crosscut by a network of veins (filled by chlorite and sericite) which usually are not propagating to the surrounding micaceous layer; **(f)** mylonitic fabric overprinted by a subvertical conjugate set of fractures (micro-graben like structure).

## Crustal shearing at ductile-brittle transition

E. Fazio et al.

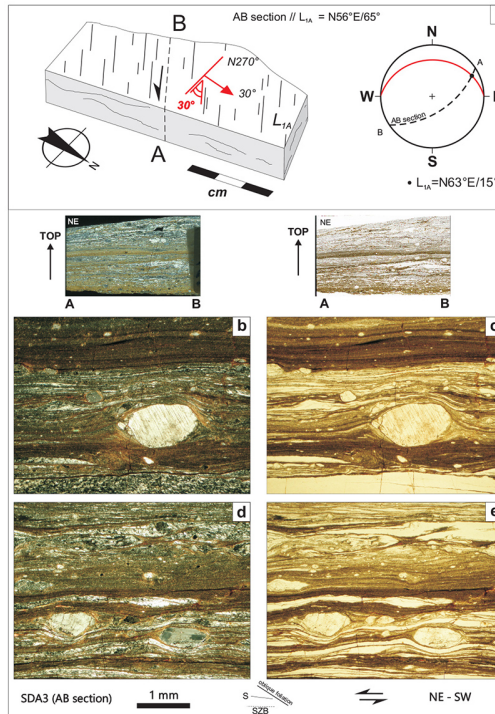


**Figure 8.** Mylonite of APU and associated microstructures (SDA3 sample – AB section): **(a)** sketching draw of oriented specimen with the trace of cut (dotted line) parallel to the stretching lineation ( $L_{1A}$ ) and relative stereonet with the mylonitic foliation ( $S_{3A}$ , red plane); **(b)** feldspar clast floating into a fine micaceous matrix (crossed polarizers); **(c)** same of **(b)** ultramylonite layer is visible in the upper part of the picture (parallel polarizers); **(d)** quartz-rich and micaceous-rich domains enveloping feldspar augens (crossed polarizers). Note the oblique foliation in the upper quartz ribbon coherent with a sinistral sense of shear (top-to-NE); **(e)** same as **(e)**, note the elongated and rounded shape of the large feldspar at the bottom-right corner (parallel polarizers).

## Crustal shearing at ductile-brittle transition

E. Fazio et al.

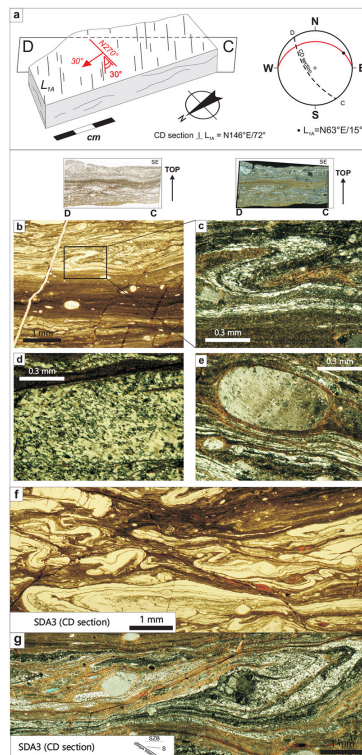


**Figure 9.** Mylonite of APU (sample SDA3 – CD thin section orthogonally cut with respect the Fig. 8): **(a)** block diagram showing thin section cut direction together with stereonet; **(b)** ultramylonite (half bottom part) interbedded with mylonite (half upper part), a set of high angle veins disrupt the horizontal foliation continuity; **(c)** detail of a (squared area) showing an intrafolial fold (crossed polarizers); **(d)** oblique foliation in quartz domain; **(e)** extremely rounded porphyroclast; **(f)** complex refolding microfabric (parallel polarizers); **(g)** complex geometry of folds affecting quartz layers (crossed polarizers).

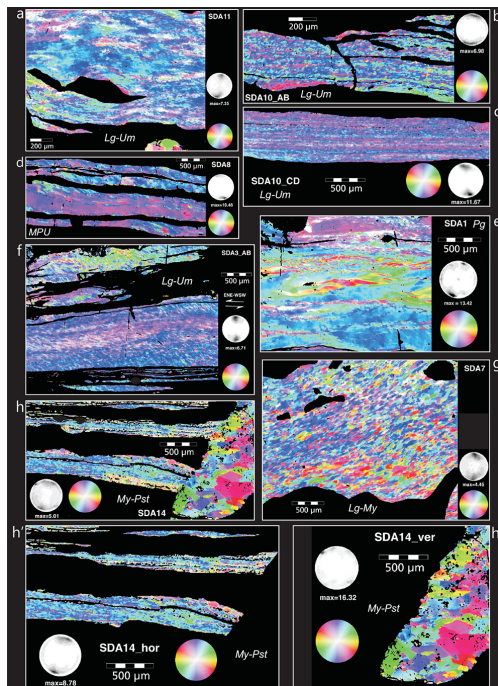


**Figure 10.** Quartz *c* axis patterns inferred by the CIP method on selected quartz-rich domains. In the crystallographic orientation images (coi) the azimuth and dip of each pixel is color coded based on the shown look-up-table: **(a)** sample SDA11; **(b)** sample SDA10 (section AB); **(c)** section SDA10 (section CD); **(d)** SDA8 sample (MPU); **(e)** SDA1 sample; **(f)** SDA3 sample (section AB); **(g)** sample SDA7; **(h)** sample SDA14: coi of a complex domain consisting of sub-horizontal syn-mylonitic quartz and post-mylonitic crosscutting subvertical quartz vein; **(h')** restricted subdomain of **(h)** focusing on the syn-shear ribbon-like quartz; **(h'')** subdomain of **(h)** showing the quartz recrystallized into the discordant vein. Legend: Pg: paragneiss; Lg: leucocratic gneiss; Um: ultramylonite; My: Mylonite; Pst: pseudotachylite; MPU: Madonna di Polsi Unit.



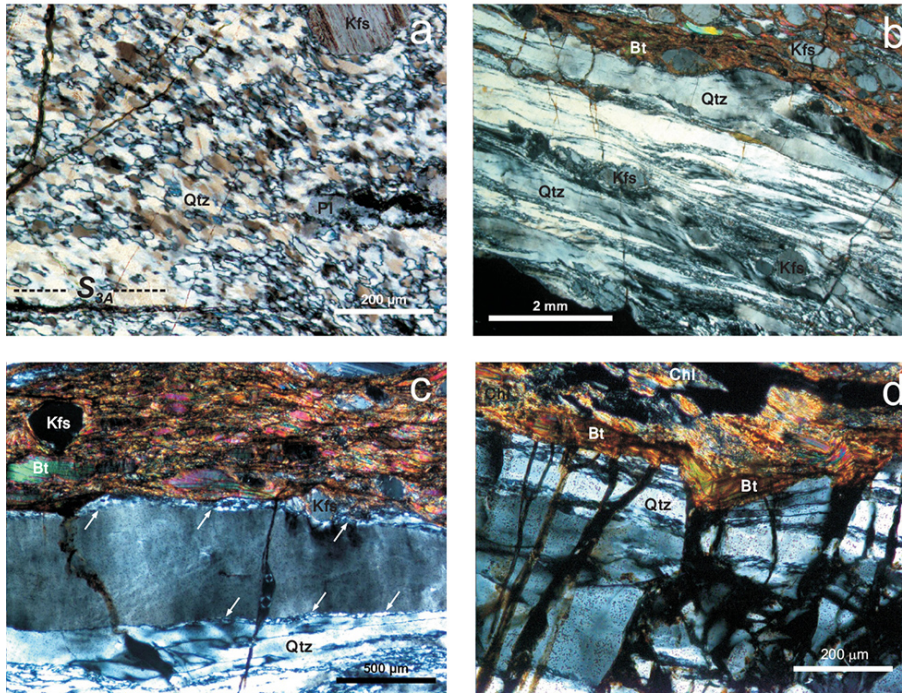


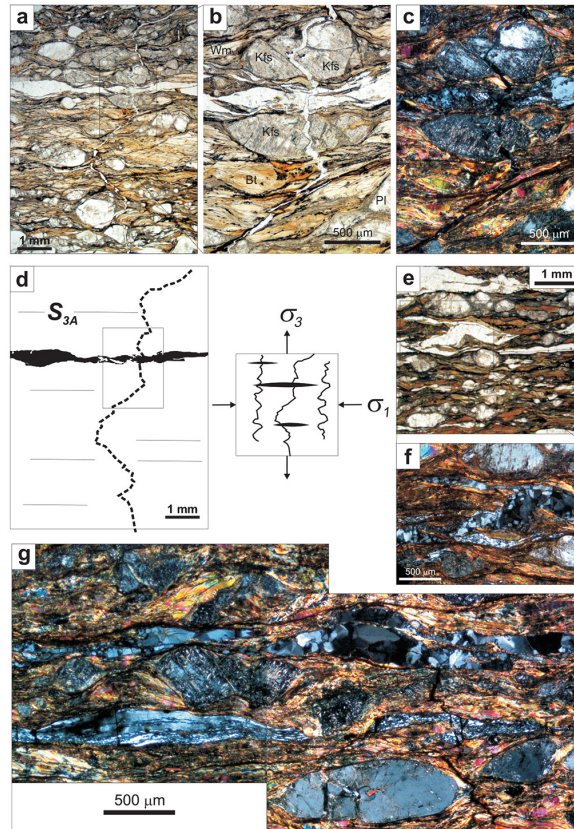
**Figure 12.** (a) Typical SGR recrystallization showing lobate grain boundaries and recrystallized grains which are slightly larger than sub grains (visible at lower left corner of the picture); (b) BLG recrystallization process showing undulose extinction of elongate grains and grain boundary bulges concentrated at the sutured edges of ribbon-like quartz; (c) undulose extinction visible within a sub-horizontal ribbon grains with associated deformation lamellae between a quartz-rich domain (lower part) and a micaceous domain (upper part) showing a mortar texture characterized by recrystallized smaller quartz grains at its margins (white arrows); (d) large quartz microlithon showing pervasive fracturing. Note here as kinking of biotite flakes are concentrated at the end of veins crosscutting the quartz layer.

# SED

7, 909–955, 2015

## Crustal shearing at ductile-brittle transition

E. Fazio et al.



Title Page

Abstract

Introduction

Conclusions

References

Tables

Figures

◀

▶

◀

▶

Back

Close

Full Screen / Esc

Printer-friendly Version

Interactive Discussion





## Crustal shearing at ductile-brittle transition

E. Fazio et al.

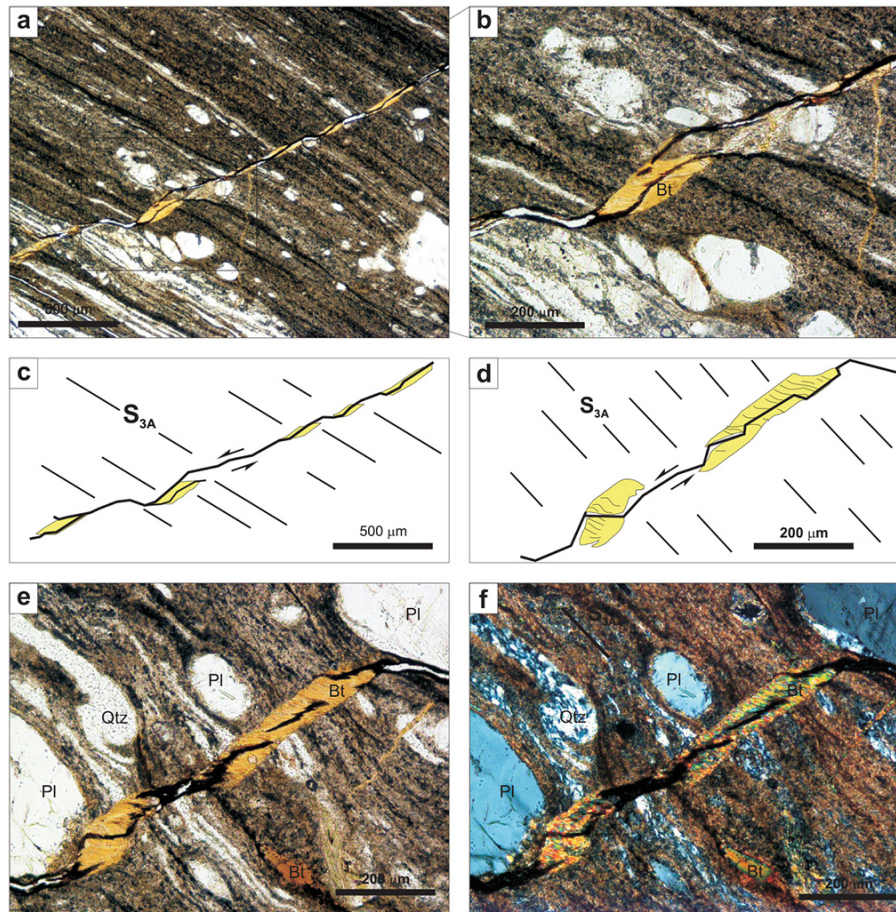


**Figure 14.** 3rd set of veins ( $V_{3A}$ ): **(a)** fibrous veins; **(b)** detail of **(a, c, d)** sketch draw of **(a, b)** respectively, suggesting a sinistral shear sense around the fracture; **(e)** other example of biotite fibrous vein; **(f)** high angle fibrous vein with respect mylonitic foliation.

Title Page

Abstract

Introduction

Conclusions

References

Tables

Figures

◀

▶

◀

▶

Back

Close

Full Screen / Esc

Printer-friendly Version

Interactive Discussion



## Crustal shearing at ductile-brittle transition

E. Fazio et al.

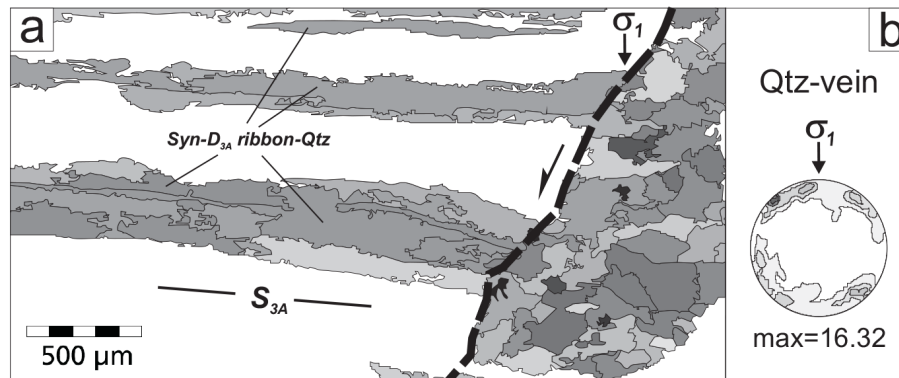


**Figure 15.** (a) Rough grain boundary map of the same domain of Fig. 9h (sample SDA14) investigated by means of the CIP method; (b) quartz  $c$  axis pattern and inferred  $\sigma_1$  orientation of the coarser quartz grains composing the vein on the right cutting at an angle of about 60 the early ribbon quartz shown on the left.

Title Page

Abstract

Introduction

Conclusions

References

Tables

Figures

◀

▶

◀

▶

Back

Close

Full Screen / Esc

Printer-friendly Version

Interactive Discussion



## Crustal shearing at ductile-brittle transition

E. Fazio et al.

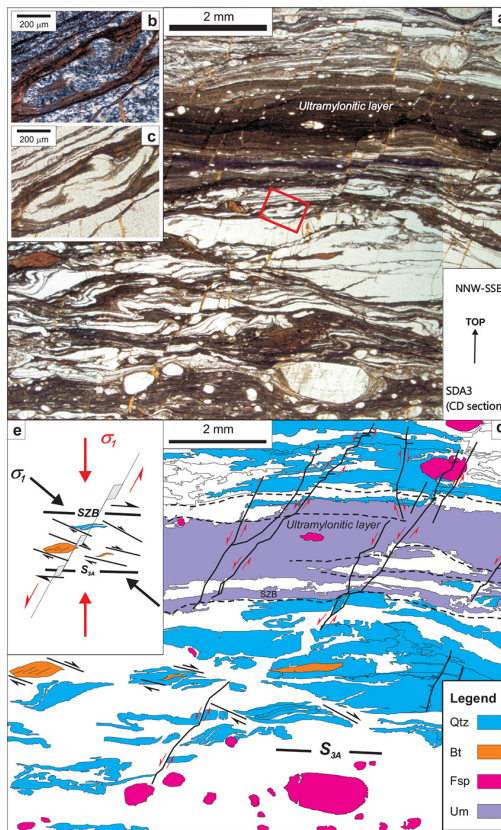


**Figure 16.** (a) Ultramylonite (sample SDA3) characterised by a complex geometry of quartz layers; (b) detail of (a) showing a complex fold (red square region near the center of the picture, crossed polarizers); (c) like (b) (parallel polarizers); (d) sketch draw with interpretation of microstructures in (a); (e) interpretative schematic draw of (d) showing superposition of ductile-regime related shear zone (black-colored  $\sigma_1$ ) and brittle-regime related veins (red-colored  $\sigma_1$ ).

Orogenic stages	Deformation phase	MESOSCOPIC FEATURES	MICROSCOPIC FEATURES	Approx. T estimates (°C)	Approx. P estimates (Gpa)
Late Apennine	D <sub>6A</sub>	<p>Normal and conjugate high angle brittle joints</p> <p>Joints <math>B_{4A}</math></p> <p><math>S_{3A} = S_{4A}</math></p> <p>1 m</p>	<p><math>\sigma_1</math></p> <p><math>S_{3A}</math></p> <p><math>\sigma_3</math></p> <p>500 <math>\mu</math>m</p>	150-250	0.1-0.2
		<p>Normal and conjugate low angle brittle joints</p> <p>Joints <math>B_{4A}</math></p> <p><math>S_{3A} = S_{4A}</math></p> <p>1 m</p>	<p><math>\sigma_3</math></p> <p><math>\sigma_1</math></p> <p>1 mm</p> <p><math>S_{3A}</math></p>		
Late Alpine	D <sub>4A</sub>	<p><math>L_{2A}</math></p> <p><math>B_{3A}</math></p> <p><math>L_{1A}</math></p> <p><math>S_{3A}</math></p> <p><math>S_{4A}</math></p> <p>10 cm</p>	<p><math>\sigma_3</math></p> <p><math>\sigma_1</math></p> <p>1 mm</p> <p><math>S_{3A}</math></p>	300-350	0.2-0.4
	M <sub>4A</sub>	Qtz+Wm <sub>1</sub> +Chl+Pl <sub>1</sub> ±Czo <sub>1</sub>			
	D <sub>3A</sub>	<p><math>L_{1A}</math></p> <p><math>S_{2A}</math></p> <p>1 cm</p>	<p><math>\sigma_1</math></p> <p><math>S_{2A}</math></p> <p>1 mm</p>		
	M <sub>3A</sub>	Qtz+Wm <sub>3</sub> +Bt+Chl <sub>3</sub> ±Pl <sub>3</sub> ±Grt <sub>3</sub> ±Czo±Tur+Amph			

**Figure 17.** Synoptic scheme illustrating the tectonic evolution of the Montalto Shear Zone also showing the linkage between mesostructural features (outcrop scale) and microscopic structures (thin section scale) during progressive deformational phases (Table 2).